ACS OMEGA

Open Access

http://pubs.acs.org/journal/acsodf

Article

Wood Fiber-Based Triboelectric Material with High Filtration Efficiency and Antibacterial Properties and Its Respiratory Monitoring in Mask

Xiaoping Sun,[§] Juan Yuan,[§] Qiuxiao Zhu, Yanfen Sun, Haoqiu Chen, Shuangli Liao, Jiaxuan Yan, Jiecheng Cai, Yuhe Wei, and Lianxin Luo*

Cite This: *ACS Omega* 2024, 9, 33643−33651

Read Online

ACCESS | Metrics & More | Article Recommendations | Supporting Information

ABSTRACT: Self-powered wearable electronic products have rapidly advanced in the fields of sensing and health monitoring, presenting greater challenges for triboelectric materials. The limited surface polarity and structural defects in wood fibers restrict their potential as substitutes for petroleum-based materials. This study used bagasse fiber as the raw material and explored various methods, including functionalizing cellulose nanofibrils (CNFs) with polydopamine (PDA), in situ embedding of silver particles, filtration, and freeze-drying. These methods aimed to enhance the triboelectric output, antibacterial properties, and filtration properties of lignocellulosic materials. The Ag/PDA/CNF-based triboelectric nanogenerator (TENG) demonstrated an open-circuit voltage of 211 V and a short-circuit current of 18.1 μA. An aerogel prepared by freeze-drying the Ag/PDA/CNF material, combined with a polyvinylidene fluoride nanofiber structure fabricated by electrospinning, constitutes the TENG unit. A self-powered respiratory detection mask was created using this combination, achieving a filtration efficiency of 94.23% for 0.3 μm particles and an antibacterial rate exceeding 99%. In addition, it effectively responded to respiratory frequency signals of slow breathing, normal breathing, and shortness of breath, with the output electrical signal correlating with the respiratory frequency. This study considerably contributes to advancing wood fiber-based triboelectric materials as alternatives to petroleum-derived materials in self-powered wearable electronic products for medical applications.

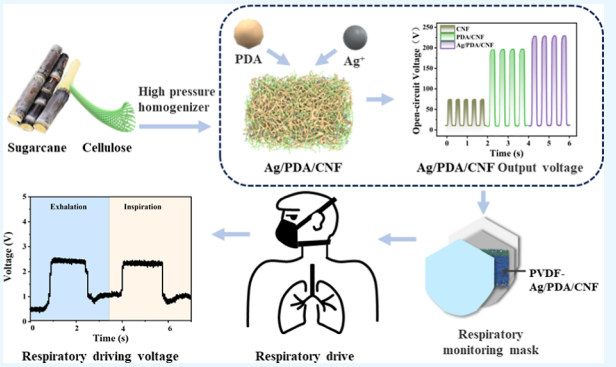

INTRODUCTION

With the rapid development of our energy-driven society, the harm caused to human health by solid particulate matter (PM) pollution has garnered widespread concern.[1−3] This is attributed to increased pollutant emissions from human activities such as transportation,[4,5] heating,[6] power plants, and industrial processes. Among PM pollutants, fine particles (PM2.5, solid particles with a diameter of 2.5 μm or less) are primarily responsible for PM-related allergies and the spread of respiratory diseases.[7−10] Filtering micron and submicron PM is time-consuming, and designing filters with ideal porous nanostructures is complex.[11,12] Masks, serving as close-fitting respiratory filtering medical protection equipment, isolate dust, waste gas, pathogenic microorganisms, and viruses. However, these masks, typically made from various plastic polymers and designed for single use, can release microplastics more easily and rapidly than plastic bottles. The emergence of nanomasks may exacerbate this effect on the nanometer scale. Although consumers may wear them for only a few hours, discarded masks can take up to 500 years to degrade. Consequently, there is growing interest in exploring environmentally friendly natural materials as substitutes for petroleum-based plastics to enhance sustainability and reduce the environmental impact. Lignocellulose, one of the most abundant renewable resources globally, is renewable, easily degradable, and low cost.[13] In addition, the abundance of hydroxyl groups[14] on the cellulose surface facilitates functionalization and modification, making it a viable green alternative to petroleum products.

The triboelectric nanogenerator (TENG), an energy-harvesting device, generates electrical signals corresponding to human respiration and can function as a self-powered health sensor without external power.[15,16] However, compared with synthetic polymers, cellulose materials exhibit weaker triboelectricity and a limited ability to generate induced charges, restricting their application in TENGs. Researchers have enhanced the frictional polarity of cellulose materials through

Received: February 27, 2024
Revised: June 7, 2024
Accepted: June 11, 2024
Published: July 26, 2024

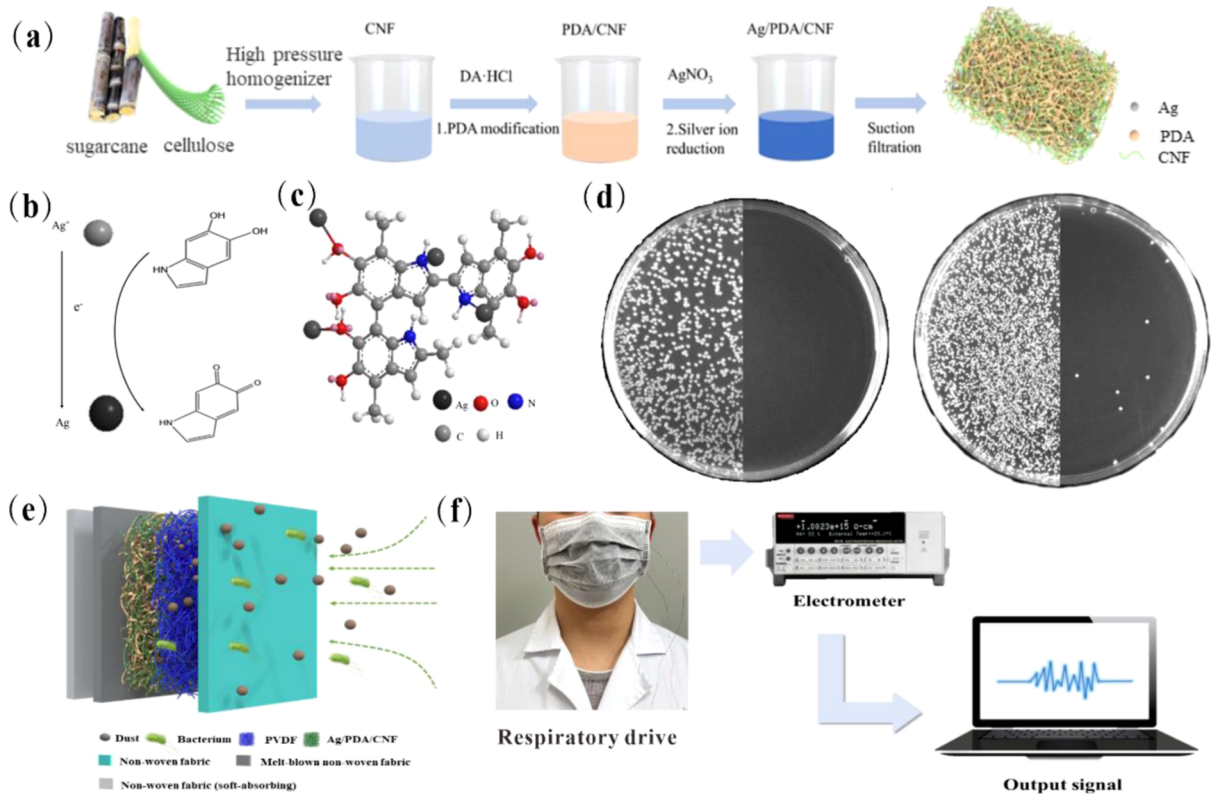

Figure 1. (a) Preparation process of Ag/PDA/CNF composites from bagasse pulp; (b) mechanism of reducing Ag^+ to Ag through PDA; (c) conceptual mechanism of the interaction between Ag and PDA; (d) comparison of antibacterial properties of Ag/PDA/CNF materials; (e) schematic diagram of particle filtration simulation of Ag/PDA/CNF + PDVF; and (f) schematic diagram of TENG driven by human breath.

chemical grafting or doping with materials possessing strong conductivity and high dielectric properties[17] to improve conductivity and charge transfer.[18−22] Luo et al.[23] prepared a low-cost cellulose aerogel TENG for self-powered smart door panels; Song et al.[24] prepared a flexible cellulose TENG material with high electrical output by grafting allicin. Ding et al.[25] prepared an integrated array structure TENG from cellulose to collect water wave energy. Polydopamine (PDA) can self-polymerize on various substrates and is widely used as a coating material.[26−28] Researchers have noted that PDA-coated surfaces contain functional groups such as hydroxyl, amino, and imine groups, which can serve as bridges for secondary modifications.[29,30] At present, metal nanoparticles functionalized with dopamine are being explored in numerous fields.[31] Silver nanoparticles (AgNPs) have a large specific surface area, small volume, excellent optical properties, and unique physical (e.g., high thermal and electrical conductivity) and chemical properties (e.g., catalytic activity), making them extensively used in optics, catalysis, biomedicine, and other fields.[32−34] Combining TENGs with particle filtration and antibacterial functions offers substantial potential for health monitoring.

In this study, we prepared a wood fiber-based triboelectric material and a self-powered respiratory detection mask, providing filtration and antibacterial capabilities. We modified nanocellulose with nontoxic, degradable, and highly biocompatible PDA and then implanted Ag nanoparticles into wood fibers via in situ reduction of Ag^+ with PDA, creating Ag/PDA/cellulose nanofibril (CNF) composites. This method enhances the triboelectric output and antibacterial properties of wood fiber. Furthermore, we used an aerogel prepared by the freeze-drying Ag/PDA/CNF material and a polyvinylidene fluoride (PVDF) nanofiber structure made via electrospinning to form a TENG unit. The resulting self-powered respiratory detection mask achieves a 94.23% filtering ability for 0.3 μm particles and responds well to respiratory frequency signals, ensuring that the output electrical signal is consistent with the respiratory frequency. This underscores the potential of self-powered wearable electronic products made from wood fiber-based triboelectric materials in medical and healthcare applications.

RESULTS AND DISCUSSION

Design Process and Effect Display of the Ag/PDA/CNF Composite Wood Fiber-Based Friction Mask Material. In Figure 1a, the process for preparing the Ag/PDA/CNF composite is depicted. At first, bleached bagasse pulp is transformed into CNFs using a high-pressure homogenizer.[35] These CNFs are subsequently modified with PDA, followed by the loading of AgNPs, filtration molding, and freeze-drying. PDA, adhering strongly to the fiber surface, possesses a crucial reducing ability capable of reducing silver ions (Ag) in situ to form AgNPs. These stable silver particles are then integrated into the lignocellulose matrix to fabricate Ag/PDA/CNF composites.[36] The aerogel, created through a combination of filtration molding and freeze-drying,[37,38] ensures a loose and porous structure, imparting flexibility and mechanical stability to the resulting sheet. Figure 1b illustrates the oxidation of the phenolic hydroxyl group in PDA to form a dopaquinone structure. The electrons generated in this process reduce Ag^+ to Ag. Figure 1c demonstrates the interaction between the Ag produced through reduction and the oxygen- and nitrogen-containing functional groups in the

https://doi.org/10.1021/acsomega.4c01906
ACS Omega 2024, 9, 33643−33651

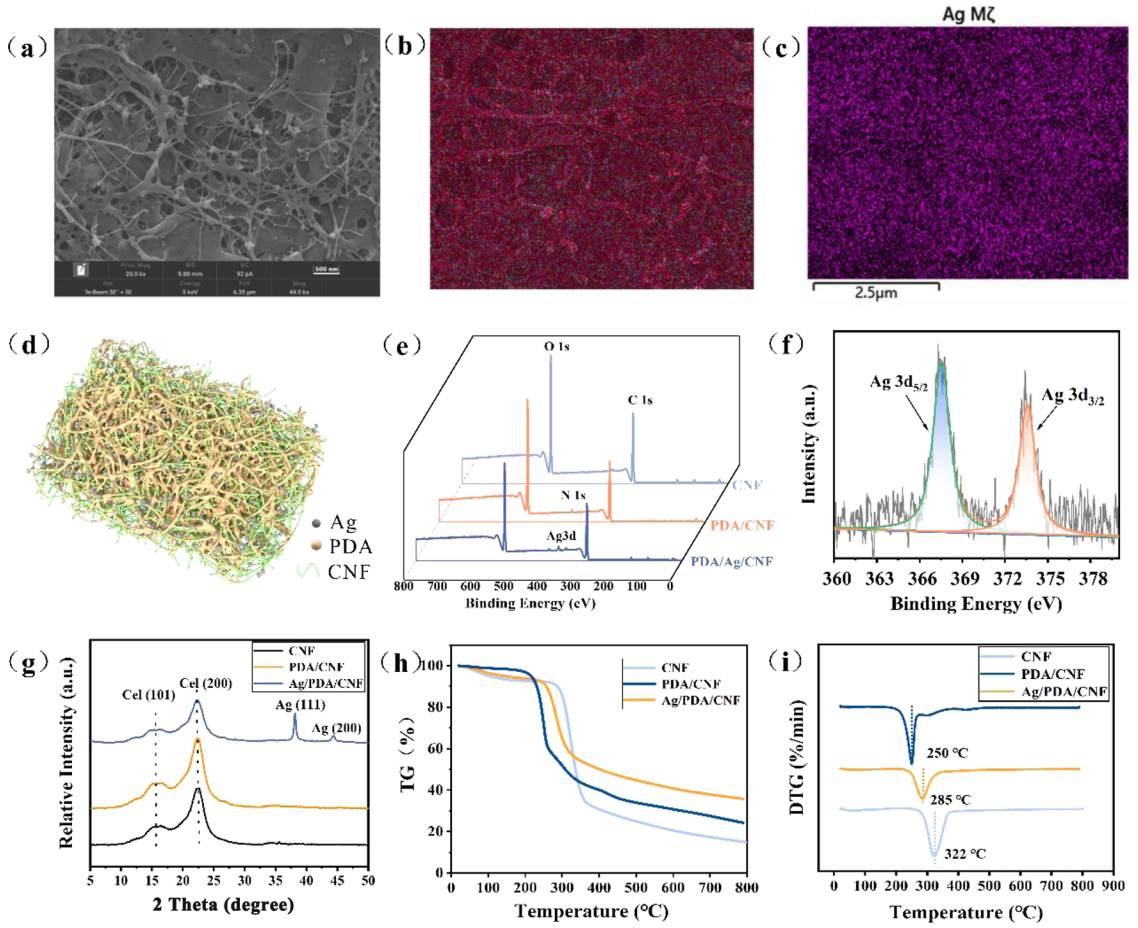

Figure 2. Micromorphology and characterization of Ag/PDA/CNF wood fiber-based triboelectric mask materials: (a) SEM images of CNF, PDA/CNF, and Ag/PDA/CNF materials; (b) full spectrum of carbon, oxygen, silver, and nitrogen in Ag/PDA/CNF materials; (c) distribution of silver in the Ag/PDA/CNF material; (d) schematic diagram describing the network structure properties of the Ag/PDA/CNF aerogel structure; (e) X-ray photoelectron spectroscopy (XPS) spectra of CNF, PDA/CNF, and Ag/PDA/CNF; (f) Ag 3d XPS spectrum of Ag/PDA/CNF; (g) X-ray diffraction (XRD) patterns of CNF, PDA/CNF, and Ag/PDA/CNF materials; and (h,i) TGA curve of CNF, PDA/CNF, and Ag/PDA/CNF.

PDA structure. This interaction is captured by dopamine, with subsequent Ag deposition on the surface of the Ag/PDA/CNF composite material, forming a Ag layer conductive network. The incorporation of metallic silver enhances the antibacterial performance of the composite efficacy against *Escherichia coli* and *Staphylococcus aureus*, as shown in Figure 1d. The Ag/PDA/CNF and PVDF multilayer composite material exhibits excellent overall filtration performance, achieving a filtration efficiency of 94.23%. This indicates that the material meets high filtration efficiency requirements, as represented in the simulated schematic of PM filtration in Figure 1e.

The Ag/PDA/CNF and PVDF membranes, when combined and integrated into a protective mask (Figure 1f), exhibit self-charging capabilities through the synergistic effects of triboelectricity and electrostatic induction. This enhancement improves the filtering efficiency. During breathing, electrical signals can be detected by an electrometer, allowing for the clear differentiation of human breathing rates based on the magnitude and frequency of these electrical signals. This holds substantial potential for applications in human respiratory monitoring.[39,40]

Micromorphology and Characterization of Ag/PDA/CNF Wood Fiber-Based Triboelectric Mask Materials. From the SEM image presented in Figure 2a, the overlapping nature of fibers in CNFs is evident, with clear fiber veins observable. PDA forms a coating on the fiber surface through a strong adhesion. Using the reducibility of dopamine, Ag^+ ions were reduced, resulting in the apparent formation of AgNPs on the surface of the composite. SEM (Figure S1a) of Ag/CNF/PDA shows that the material has a porous structure. EDS analysis of Ag/PDA/CNF, as depicted in Figure 2b,c, reveals a widespread distribution of the Ag elements within the composite material. A network structure of silver particles forms along the fiber veins, and the proportion of Ag elements is 6.35%. This indicates a high loading capacity and uniformity of Ag on the surface of cellulose fibers. The catechol group of PDA chelates Ag^+, providing a uniform and stable anchoring point for Ag on cellulose. This allows PDA to strongly regulate the loading state of Ag on the fiber, effectively preventing aggregation. Figure 2d illustrates the schematic diagram of the network structure properties of Ag in aerogels.[41,42]

Figure 2e,f shows that after in situ reduction of silver ions, a new Ag 3d binding energy peak appears in the Ag/PDA/CNF spectrum. Analyzing the Ag 3d peaks in Figure 2g, it is observed that Ag 3d distributes between Ag $3d_{5/2}$ and Ag $3d_{3/2}$, with binding energies of 367.4 and 373.6 eV, respectively. The presence of zerovalent Ag on the PDA surface is indicated by an energy difference of 5.8 eV. The characteristic peak of Ag 3d corresponds to the Ag element in EDS, confirming that Ag^+ is reduced by PDA to form Ag. These spectra and diffraction

https://doi.org/10.1021/acsomega.4c01906
ACS Omega 2024, 9, 33643−33651

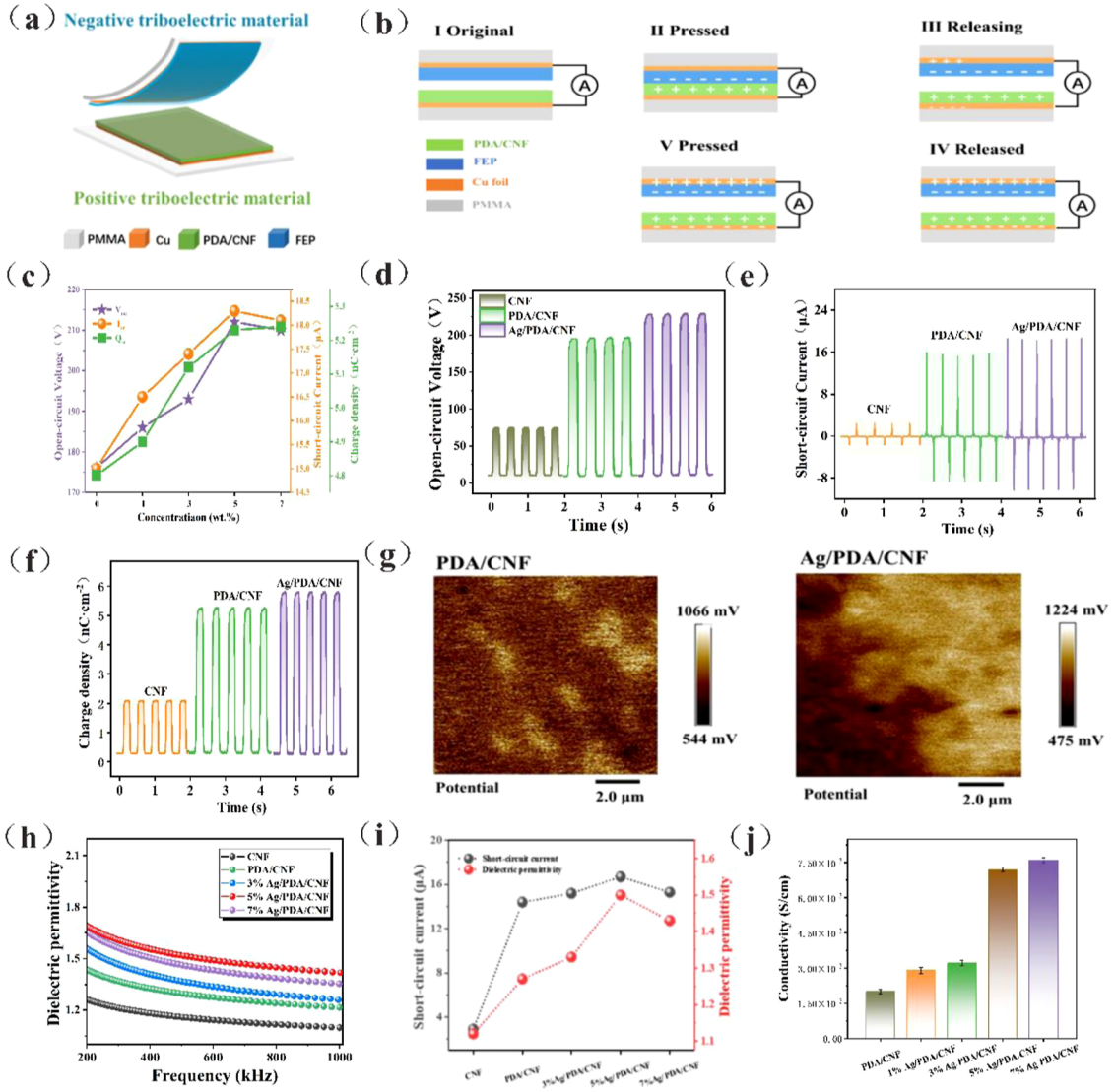

Figure 3. Triboelectric output performance and enhancement mechanism of Ag/PDA/CNF. (a) Configuration of the Ag/PDA/CNF-TENG device; (b) basic principle diagram of the PDA/CNF-TENG power generation process; (c) changes in V_{oc}, I_{sc}, and Q_{sc} of TENG with different Ag contents; the composite material outputs (d) voltage, (e) current, and (f) charge density at a frequency of 2 Hz; the enhancement mechanism of TENG's output performance: (g) comparison of surface potential of CNF and Ag/PDA/CNF composites; (h) variation in the dielectric constant of Ag/PDA/CNF composites with different Ag contents vs frequency at room temperature; (i) short-circuit current; and (j) electrical conductivity of Ag/PDA/CNF composites.

analyses provide conclusive evidence for the in situ doping of Ag^+ into the wood fiber composite matrix.[43,44] Figure 2g indicates that CNFs and the composite retain the typical diffraction peaks of cellulose[45] at 16.2 and 22.3, whereas the Ag/PDA/CNF composites exhibit diffraction peaks of Ag at 38.2 and 44.2, corresponding to the crystal planes of cubic silver crystals (111) and (200), respectively. The intensity of the crystal plane (111) is more pronounced. It was found that the degradation of PDA/CNF and Ag/PDA/CNF composites was earlier than that of CNF due to the addition of PDA (Figure 2h,i).

Detection of Triboelectric Properties, Filtration Properties, and Antibacterial Properties of Ag/PDA/CNF. Figure 3a,b illustrate the schematic diagrams of Ag/PDA/CNF-TENG. This device employs an Ag/PDA/CNF composite as the positive friction material and an FEP film as the negative friction material. The triboelectric properties of the TENG were evaluated by using this configuration. The fundamental principle of operation is based on the synergistic effect of triboelectric and electrostatic induction occurring during the contact separation process of the positive and negative triboelectric materials.

In Figure 3c, Ag/PDA/CNF with a 5% Ag content exhibits the best output performance. Figure 3d−f depicts the changing trends in the electrical output performance of the 5% Ag/PDA/CNF. Compared with the CNF film, the open-circuit voltage, short-circuit current, and transfer charge have increased by 245% (from 64 to 221 V), 624% (from 2.5 to 18.1 μA), and 733% (from 1.8 to 15 nC), respectively. In comparison with the PDA/CNF composite film, these values have increased by 14.1% (from 191 to 221 V), 15.3% (from 15.33 to 18.1 μA), and 12.1% (from 13.2 to 15 nC). This indicates that the triboelectric properties of lignocellulose are enhanced by the integration of silver particles.

The surface potential of Ag/PDA/CNF, at 1069 mV, is 13% higher than that of the PDA/CNF composite (946 mV), as

https://doi.org/10.1021/acsomega.4c01906
ACS Omega 2024, 9, 33643−33651

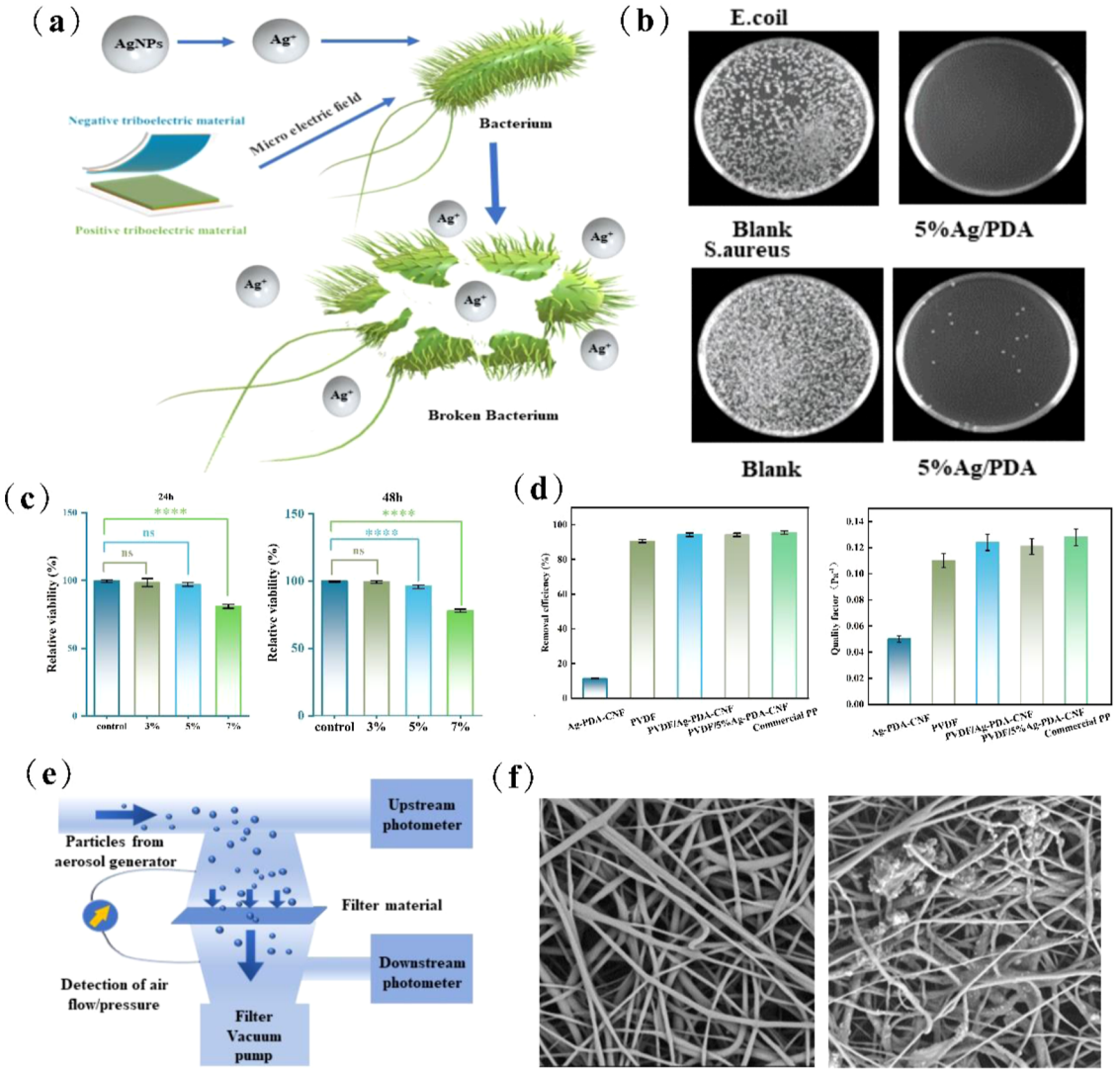

Figure 4. Detection of filtration performance and antibacterial performance of the wood fiber-based friction electric mask material Ag/PDA/CNF. (a) Schematic diagram of the sterilization mechanism of the Ag/PDA/CNF composite material; (b) antibacterial properties of Ag/PDA/CNF; (c) cell viability of the Ag/PDA/CNF composite cocultured with HUVECs for 24 and 48 h; (d) filtration efficiency and filtration quality factor of the Ag/PDA/CNF composite; (e) simulation schematic of Ag/PDA/CNF for PM filtration; and (f) SEM images of the PVDF membrane surface before and after filtration.

shown in Figure 3g. This demonstrates that the triboelectric positive polarity of the material is effectively improved by silver particles. The conductivity of Ag/PDA/CNF is noticeably higher than that of PDA/CNF, as illustrated in Figure 3h. This increase in conductivity accelerates the production and transfer efficiency of the charge. The addition of silver particles leads to an increase in the dielectric constant of the material (Figure 3h), enhancing the surface material's charge storage capacity, which is advantageous for the improvement of TENG output performance. The correlation between the dielectric properties of the material and the output current is presented in Figure 3i,j. The I_{sc} current of the Ag/PDA/CNF composites rises with an increase in the dielectric properties of the material. The augmented dielectric constant of the matrix results in the concentration of numerous nanoparticles in the electric field, aiding in capturing more electrons and considerably enhancing the surface charge density.

The schematic diagram illustrating the sterilization mechanism of Ag/PDA/CNF is depicted in Figure 4a. In addition to the antibacterial effect of Ag, its antibacterial performance encompasses a microelectric field antibacterial effect produced by the redox reaction. The potential antibacterial mechanisms of the microelectric field include the following: (1) electrical stimulation disrupts the bacterial membrane, leading to the loss of vital components within the membrane and (2) the electrolytic reaction induced by electrical stimulation generates toxic substances (reactive oxygen species) that eradicate bacteria.[46−48]

Figure 4b shows the antibacterial effects of Ag/PDA/CNF against *E. coli* and *S. aureus*. The antibacterial rates for both are over 99%, indicating that Ag/PDA/CNF possesses exceptional antibacterial properties. The comparison between the bacteriostatic standard of medical mask and the bacteriostatic performance of Ag/PDA/CNF mask material (Figure S2) shows that the material has reached the bacteriostatic standard of medical mask.[49] The cell viability of HUVECs cultured for 24 and 48 h, as shown in Figure 4c, was 97.12 and 95.31%, respectively. According to the toxicity classification method of the United States Pharmacopoeia, the cytotoxicity of the 5% Ag/PDA/CNF samples was deemed nontoxic to HUVECs.

https://doi.org/10.1021/acsomega.4c01906
ACS Omega 2024, 9, 33643−33651

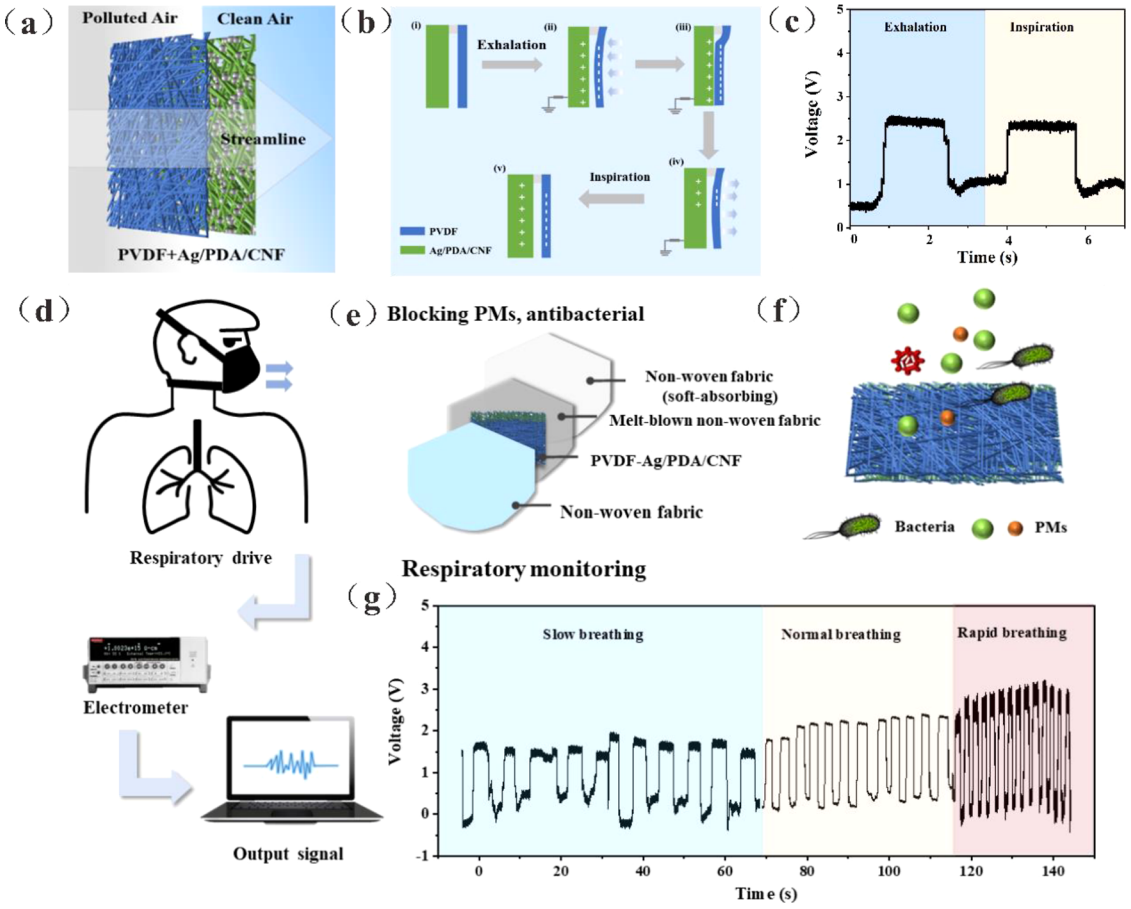

Figure 5. (a) Assembly and application of TENG assembly of Ag/PDA/CNF composites and PVDF materials, (b) TENG's working mechanism, and (c) voltage signal driven by respiration; (d) TENG process driven by human breath; (e) schematic diagram of the filtering structure the mask; (f) schematic diagram of the filtering function of the mask; and (g) respiratory output electrical signals with different frequencies.

This experiment substantiates its safety for use in personal protective devices.

The simulation diagram of Ag/PDA/CNF for PM filtration is displayed in Figure 4d. The filtration performance of the material for 0.3 μm particles was evaluated, as shown in Figure 4e. The filtration efficiency of PDVF and the 5% Ag/PDA/CNF composite reached 94.23%, comparable to that of a commercial polypropylene melt-blown cloth (95.48%). This indicates that the material fulfills the criteria for a high filtration efficiency. Moreover, its quality factor value is considerably superior to that of PVDF, demonstrating excellent overall filtration performance.[50]

Application of Ag/PDA/CNF Assembly TENG. The TENG, assembled using Ag/PDA/CNF and PVDF, is shown in Figure 5a. The airflow generated by breathing periodically causes the Ag/PDA/CNF aerogels and PVDF nanofibers to contact and separate from each other, as shown in Figure 5b. This action drives the TENG to produce induced charges and generates a voltage peak in a breathing cycle, as shown in Figure 5c. The frequency of the electrical signals is consistent with the breathing frequency. The TENG's electrical signal (voltage) is collected and processed by an electrometer and then outputted through a computer, as demonstrated in Figure 5d. When this antibacterial material is incorporated into a protective mask (Figure 5e), it not only provides physical filtration to remove particles and bacteria, as shown in Figure 5f, but is also driven by breath to generate induced charge. Figure 5g displays the voltage signals at the breathing frequencies of slow, normal, and rapid breathing, showing distinct changes corresponding to different breathing states. And different batches of mask materials also have good consistency (Figure S3), and the effects of temperature and humidity on electrical signals (Figure S4) and stability[51] (Figure S5) were measured. The frequency of the voltage signal can indicate the speed of breathing, but the voltage during normal breathing is similar to that during slow breathing, primarily because of minimal differences in breathing intensity.[52] Consequently, the test demonstrates that the TENG's protective mask made of Ag/PDA/CNF can monitor the breathing state of the human body.

CONCLUSIONS

Against the backdrop of current resource scarcity and environmental pollution, the transformation of abundant cellulose resources in nature into advanced functional materials to meet the urgent need for human health is becoming increasingly apparent. This study prepared a high-efficiency, antibacterial wood-based TENG material, Ag/PDA/CNF composite film, and explored its frictional electricity output performance. It was found that the output voltage reached 211 V, the short-circuit current was 18.1 μA, and the power density was 60.06 μW/cm^2. By combination of the Ag/PDA/CNF composite film with a PVDF layer, a self-powered respiratory monitoring mask was developed. The TENG output signals of the mask demonstrated good consistency with breathing

https://doi.org/10.1021/acsomega.4c01906
ACS Omega 2024, 9, 33643−33651

frequency, achieving a filtration efficiency of 94.23% and exhibiting significant antibacterial properties, thus making it safe for use in personal protective mask materials. This study demonstrates the excellent antibacterial, filtration, and respiratory monitoring effects of wood-based materials, highlighting the enormous potential of wood-based triboelectric materials as replacements for petroleum-derived materials in the application of self-powered wearable electronic products.

EXPERIMENTAL SECTION

Materials. Bagasse cellulose fiber was supplied by Guangxi Chongzuo East Asia Sugar Co., Ltd. (Nanning, China) and homogenized with a high-pressure homogenizer to obtain CNFs.

Preparation of Ag/PDA/CNF Aerogels. Weighed 0.1 g portion of tris(hydroxymethyl)aminomethane and 0.5 g of CNFs were dispersed into 100 mL of distilled water. The pH was adjusted to 8.5 using 0.1 mol/L HCl and 0.1 mol/L NaOH solutions. Subsequently, 24 mg of dopamine hydrochloride (DA·HCl) was weighed and dissolved in this solution. The suspension was then closed and kept in the dark for 2 h, forming PDA/CNF. When 0.4225 g of a standard solution of silver nitrate was added to the suspension for 2 h, PDA, due to its strong reducing ability, reduced silver nitrate in situ to form AgNPs. After the reaction, the samples were washed, and Ag/PDA/CNF aerogel composites were obtained by freeze-drying, with no toxic reagents involved in the process.

Preparation of the PVDF Fiber Membrane. The PVDF fiber membrane was prepared by electrospinning. Here, 4.0 g of PVDF was dissolved in 20 mL of *N*,*N*-dimethylformamide and heated and stirred in a water bath at 70 °C until it was fully dissolved. The solution was then transferred to a syringe. The applied voltage was set to 15 kV, the humidity to 45% RH, the temperature to 25 °C, and the spinning speed to 2 mL/h. After being spun, the obtained fiber membrane was dried in a vacuum oven for 12 h.

The surface morphology of the Ag/PDA/CNF composite film was observed by using field emission scanning electron microscopy (FE-SEM, S-3400N, Japan), and the content of surface elements was determined by its accessory energy spectrometer. XPS (ESCALAB 250XI+, Los Angeles, USA) was used to analyze the basic characteristics of Ag/PDA/CNF materials. XRD (MINFLEX600, Songjiang, Japan) was employed to study the crystal structure, with a scanning speed of 3°/min and a range of 5−50°. A linear motor (P01-37 × 120-C, Guangdong, China) generated different frequencies, and the output performance of the TENG was measured by using an electrometer (Keithley 6514, Ohio, USA) and an acquisition card (NI-USB-6259, Houston, USA).

Preparation of PVDF-Ag/PDA/CNF-Based TENG. The Ag/PDA/CNF aerogel and PVDF membrane were cut into rectangles measuring 10 cm × 5 cm and incorporated into a protective mask. Owing to the inherent conductivity of the Ag/PDA/CNF composite, it also functioned as the electrode material for the TENG. A copper wire was connected from the Ag/PDA/CNF side to an external circuit, and the electrical signal data was recorded using an electrometer.

Ag/PDA/CNF Material Antibacterial and Cytotoxicity Tests to HUVECs. The antibacterial activity of the Ag/PDA/CNF material against *S. aureus* and *E. coli* was evaluated according to the JIS Z 2801 standard. A blank control group consisted of a diluted bacterial solution, and each test was replicated thrice. Cytotoxicity was assessed per ISO standard 10993, evaluating the cytotoxicity of materials to HUVECs using the CCK-8 method. HUVECs were cultured in a Dulbecco modified Eagle's medium containing 10% fetal bovine serum at 37 °C and 5% CO_2.

Material Filtration Performance Test. The filtration efficiency and pressure drop of the material were tested by using an automatic filter material detector. The effective test area was set at 200 cm^2. Neutral dispersed NaCl solid aerosol with a mass median diameter of 0.30 ± 0.06 μm was directed onto the fiber membrane for testing. Tests were conducted at 25 °C, with a gas flow rate controlled at 32 L ± 1 L/min, and each filtration test was 1 min.

Self-Powered TENG Respiratory Monitoring. The Ag/PDA/CNF aerogels and PVDF membranes were integrated into the protective mask, enabling the TENG to be activated by respiratory airflow, thus generating a triboelectric effect. Leveraging its antibacterial and filtration capabilities, the induced charges were used for respiratory sensing. The generated charges were collected by an electrometer to produce electrical signals, allowing for the observation of changes in respiratory frequency and intensity.

ASSOCIATED CONTENT

Supporting Information

The Supporting Information is available free of charge at https://pubs.acs.org/doi/10.1021/acsomega.4c01906.

SEM image of material section; comparison of antibacterial properties between medical mask and Ag/PDA/CNF mask materials; comparison chart of electrical properties of different batches of materials; electrical output performance of Ag/PDA/CNF-PVDF TENG at S5 different temperatures and humidity; and Ag/CNF/PDA-PVDF TENG stability test (PDF)

AUTHOR INFORMATION

Corresponding Author

Lianxin Luo − *Guangxi Key Laboratory of Clean Pulp & Papermaking and Pollution Control, School of Light Industry and Food Engineering, Guangxi University, Nanning 530004, China; Industrial and Food Engineering, Guangxi University, Nanning 530004, China;* orcid.org/0000-0001-9699-3155; Email: luolianxin@gxu.edu.cn

Authors

Xiaoping Sun − *Guangxi Key Laboratory of Clean Pulp & Papermaking and Pollution Control, School of Light Industry and Food Engineering, Guangxi University, Nanning 530004, China; Industrial and Food Engineering, Guangxi University, Nanning 530004, China*

Juan Yuan − *Guangxi Key Laboratory of Clean Pulp & Papermaking and Pollution Control, School of Light Industry and Food Engineering, Guangxi University, Nanning 530004, China; Industrial and Food Engineering, Guangxi University, Nanning 530004, China*

Qiuxiao Zhu − *Guangxi Key Laboratory of Clean Pulp & Papermaking and Pollution Control, School of Light Industry and Food Engineering, Guangxi University, Nanning 530004, China; Industrial and Food Engineering, Guangxi University, Nanning 530004, China*

Yanfen Sun − *Guangxi Key Laboratory of Clean Pulp & Papermaking and Pollution Control, School of Light Industry*

https://doi.org/10.1021/acsomega.4c01906
ACS Omega 2024, 9, 33643−33651

and Food Engineering, Guangxi University, Nanning 530004, China; Industrial and Food Engineering, Guangxi University, Nanning 530004, China

Haoqiu Chen − *Guangxi Key Laboratory of Clean Pulp & Papermaking and Pollution Control, School of Light Industry and Food Engineering, Guangxi University, Nanning 530004, China; Industrial and Food Engineering, Guangxi University, Nanning 530004, China*

Shuangli Liao − *Guangxi Key Laboratory of Clean Pulp & Papermaking and Pollution Control, School of Light Industry and Food Engineering, Guangxi University, Nanning 530004, China; Industrial and Food Engineering, Guangxi University, Nanning 530004, China*

Jiaxuan Yan − *Guangxi Key Laboratory of Clean Pulp & Papermaking and Pollution Control, School of Light Industry and Food Engineering, Guangxi University, Nanning 530004, China; Industrial and Food Engineering, Guangxi University, Nanning 530004, China*

Jiecheng Cai − *Guangxi Key Laboratory of Clean Pulp & Papermaking and Pollution Control, School of Light Industry and Food Engineering, Guangxi University, Nanning 530004, China; Industrial and Food Engineering, Guangxi University, Nanning 530004, China*

Yuhe Wei − *Guangxi Key Laboratory of Clean Pulp & Papermaking and Pollution Control, School of Light Industry and Food Engineering, Guangxi University, Nanning 530004, China; Industrial and Food Engineering, Guangxi University, Nanning 530004, China*

Complete contact information is available at: https://pubs.acs.org/10.1021/acsomega.4c01906

Author Contributions

[§]X.S. and J.Y. contributed to this work equally.

Notes

The authors declare no competing financial interest.

■ ACKNOWLEDGMENTS

This research was supported by the National Natural Science Foundation of China (22368008). We thank the Guangxi Key Laboratory of Clean Pulp & Papermaking and Pollution Control for providing the technology and financial support. The authors would like to thank Shiyanjia Lab for the support of XPS analysis.

■ REFERENCES

(1) Cai, R.-R.; Zhang, L.-Z. Progress and perspective of polymer electret-based PM2.5 filtration: Efficiencies, regeneration, and energy implications. *Energy* **2023**, *283*, 128504.

(2) Jeong, S.; Cho, H.; Han, S.; Won, P.; Lee, H.; Hong, S.; Yeo, J.; Kwon, J.; Ko, S. H. High Efficiency, Transparent, Reusable, and Active PM2.5 Filters by Hierarchical Ag Nanowire Percolation Network. *Nano Lett.* **2017**, *17* (7), 4339−4346.

(3) Thangavel, P.; Park, D.; Lee, Y. C. Recent Insights into Particulate Matter (PM(2.5))-Mediated Toxicity in Humans: An Overview. *Int. J. Environ. Res. Public Health* **2022**, *19* (12), 7511.

(4) Mousavinezhad, S.; Choi, Y.; Khorshidian, N.; Ghahremanloo, M.; Momeni, M. Air quality and health co-benefits of vehicle electrification and emission controls in the most populated United States urban hubs: Insights from New York, Los Angeles, Chicago, and Houston. *Sci. Total Environ.* **2024**, *912*, 169577.

(5) He, L.; Li, G.; Wu, X.; Zhang, S.; Tian, M.; Li, Z.; Huang, C.; Hu, Q.; Wu, Y.; Hao, J. Characteristics of NO(X) and NH(3) emissions from in-use heavy-duty diesel vehicles with various aftertreatment technologies in China. *J. Hazard. Mater.* **2024**, *465*, 133073.

(6) Chen, L.; Zhang, F.; Ren, J.; Li, Z.; Xu, W.; Sun, Y.; Liu, L.; Wang, X. Changes in wintertime visibility across China over 2013−2019 and the drivers: A comprehensive assessment using machine learning method. *Sci. Total Environ.* **2024**, *912*, 169516.

(7) Zhang, Y.; Zhu, Z.; Wang, W.-N.; Chen, S.-C. Mitigating the relative humidity effects on the simultaneous removal of VOCs and PM2.5 of a metal-organic framework coated electret filter. *Sep. Purif. Technol.* **2022**, *285*, 120309.

(8) Qi, Z.; Song, Y.; Ding, Q.; Liao, X.; Li, R.; Liu, G.; Tsang, S.; Cai, Z. Water soluble and insoluble components of PM(2.5) and their functional cardiotoxicities on neonatal rat cardiomyocytes in vitro. *Ecotoxicol. Environ. Saf.* **2019**, *168*, 378−387.

(9) Henning, R. J. Particulate Matter Air Pollution is a Significant Risk Factor for Cardiovascular Disease. *Curr. Probl. Cardiol.* **2024**, *49* (1), 102094.

(10) Krittanawong, C.; Qadeer, Y. K.; Hayes, R. B.; Wang, Z.; Thurston, G. D.; Virani, S.; Lavie, C. J. PM(2.5) and cardiovascular diseases: State-of-the-Art review. *Int. J. Cardiol. Cardiovasc. Risk Prev.* **2023**, *19*, 200217.

(11) Chen, C. F.; Hsu, C. H.; Chang, Y. J.; Lee, C. H.; Lee, D. L. Efficacy of HEPA Air Cleaner on Improving Indoor Particulate Matter 2.5 Concentration. *Int. J. Environ. Res. Public Health* **2022**, *19* (18), 11517.

(12) Bian, Y.; Wang, S.; Zhang, L.; Chen, C. Influence of fiber diameter, filter thickness, and packing density on PM2.5 removal efficiency of electrospun nanofiber air filters for indoor applications. *Build. Environ.* **2020**, *170*, 106628.

(13) Hui, Z.; Zhang, L.; Ren, G.; Sun, G.; Yu, H. D.; Huang, W. Green Flexible Electronics: Natural Materials, Fabrication, and Applications. *Adv. Mater.* **2023**, *35* (28), No. e2211202.

(14) Chang, S.; Weng, Z.; Zhang, C.; Jiang, S.; Duan, G. Cellulose-Based Intelligent Responsive Materials: A Review. *Polymers* **2023**, *15* (19), 3905.

(15) Mo, J.; Zhang, C.; Lu, Y.; Liu, Y.; Zhang, N.; Wang, S.; Nie, S. Radial piston triboelectric nanogenerator-enhanced cellulose fiber air filter for self-powered particulate matter removal. *Nano Energy* **2020**, *78*, 105357.

(16) Fan, F.-R.; Tian, Z.-Q.; Lin Wang, Z. Flexible triboelectric generator. *Nano Energy* **2012**, *1* (2), 328−334.

(17) Du, G.; Wang, J.; Liu, Y.; Yuan, J.; Liu, T.; Cai, C.; Luo, B.; Zhu, S.; Wei, Z.; Wang, S.; Nie, S. Fabrication of Advanced Cellulosic Triboelectric Materials via Dielectric Modulation. *Adv. Sci.* **2023**, *10* (15), No. e2206243.

(18) Zhang, C.; Lin, X.; Zhang, N.; Lu, Y.; Wu, Z.; Liu, G.; Nie, S. Chemically functionalized cellulose nanofibrils-based gear-like triboelectric nanogenerator for energy harvesting and sensing. *Nano Energy* **2019**, *66*, 104126.

(19) Yao, C.; Yin, X.; Yu, Y.; Cai, Z.; Wang, X. Chemically Functionalized Natural Cellulose Materials for Effective Triboelectric Nanogenerator Development. *Adv. Funct. Mater.* **2017**, *27* (30), 1700794.

(20) He, X.; Zou, H.; Geng, Z.; Wang, X.; Ding, W.; Hu, F.; Zi, Y.; Xu, C.; Zhang, S. L.; Yu, H.; Xu, M.; Zhang, W.; Lu, C.; Wang, Z. L. A Hierarchically Nanostructured Cellulose Fiber-Based Triboelectric Nanogenerator for Self-Powered Healthcare Products. *Adv. Funct. Mater.* **2018**, *28* (45), 1805540.

(21) Zhang, C.; Mo, J.; Fu, Q.; Liu, Y.; Wang, S.; Nie, S. Wood-cellulose-fiber-based functional materials for triboelectric nanogenerators. *Nano Energy* **2021**, *81*, 105637.

(22) Luo, B.; Cai, C.; Liu, T.; Zhang, S.; Gao, C.; Liu, Y.; Chi, M.; Wang, J.; Wang, S.; Nie, S. Triboelectric probes for investigating charge transfer at the colloid-solid interface. *Nano Energy* **2023**, *117*, 108874.

(23) Luo, C.; Ma, H.; Yu, H.; Zhang, Y.; Shao, Y.; Yin, B.; Ke, K.; Zhou, L.; Zhang, K.; Yang, M.-B. Enhanced Triboelectric Nanogenerator Based on a Hybrid Cellulose Aerogel for Energy Harvesting

and Self-Powered Sensing. *ACS Sustainable Chem. Eng.* **2023**, *11* (25), 9424−9432.
(24) Song, J. M.; Latif, M.; Jiang, Y.; Ounaies, Z.; Kim, J. High-performance flexible triboelectric nanogenerator based on micro-patterned allicin-grafted cellulose film. *Materials Today Nano* **2024**, *26*, 100475.
(25) Ding, Z.; Tian, Z.; Ji, X.; Wang, D.; Ci, X.; Shao, X.; Rojas, O. J. Cellulose-based superhydrophobic wrinkled paper and electrospinning film as green tribolayer for water wave energy harvesting. *Int. J. Biol. Macromol.* **2023**, *234*, 122903.
(26) Ruppel, S. S.; Liang, J. Tunable Properties of Polydopamine Nanoparticles and Coated Surfaces. *Langmuir* **2022**, *38* (16), 5020−5029.
(27) Beckford, S.; Mathurin, L.; Chen, J.; Fleming, R. A.; Zou, M. The effects of polydopamine coated Cu nanoparticles on the tribological properties of polydopamine/PTFE coatings. *Tribol. Int.* **2016**, *103*, 87−94.
(28) Goh, S. C.; Luan, Y.; Wang, X.; Du, H.; Chau, C.; Schellhorn, H. E.; Brash, J. L.; Chen, H.; Fang, Q. Polydopamine-polyethylene glycol-albumin antifouling coatings on multiple substrates. *J. Mater. Chem. B* **2018**, *6* (6), 940−949.
(29) Sun, Q.; Wang, L.; Yue, X.; Zhang, L.; Ren, G.; Li, D.; Wang, H.; Han, Y.; Xiao, L.; Lu, G.; Yu, H.-D.; Huang, W. Fully sustainable and high-performance fish gelatin-based triboelectric nanogenerator for wearable movement sensing and human-machine interaction. *Nano Energy* **2021**, *89*, 106329.
(30) Yang, H.-C.; Luo, J.; Lv, Y.; Shen, P.; Xu, Z.-K. Surface engineering of polymer membranes via mussel-inspired chemistry. *J. Membr. Sci.* **2015**, *483*, 42−59.
(31) Banerjee, K.; Ravishankar Rai, V. A Review on Mycosynthesis, Mechanism, and Characterization of Silver and Gold Nanoparticles. *BioNanoScience* **2018**, *8* (1), 17−31.
(32) Almajhdi, F. N.; Fouad, H.; Khalil, K. A.; Awad, H. M.; Mohamed, S. H.; Elsarnagawy, T.; Albarrag, A. M.; Al-Jassir, F. F.; Abdo, H. S. In-vitro anticancer and antimicrobial activities of PLGA/silver nanofiber composites prepared by electrospinning. *J. Mater. Sci.: Mater. Med.* **2014**, *25* (4), 1045−1053.
(33) Beltran Pineda, M. E.; Lizarazo Forero, L. M.; Sierra, Y. C. A. Mycosynthesis of silver nanoparticles: a review. *BioMetals* **2023**, *36* (4), 745−776.
(34) Xu, Z.; Zha, X.; Ji, R.; Zhao, H.; Zhou, S. Green Biosynthesis of Silver Nanoparticles Using Aqueous Extracts of Ageratum Conyzoides and Their Anti-Inflammatory Effects. *ACS Appl. Mater. Interfaces* **2023**, *15*, 13983−13992.
(35) Hassan, S. S.; Williams, G. A.; Jaiswal, A. K. Emerging technologies for the pretreatment of lignocellulosic biomass. *Bioresour. Technol.* **2018**, *262*, 310−318.
(36) Niyonshuti, I. I.; Krishnamurthi, V. R.; Okyere, D.; Song, L.; Benamara, M.; Tong, X.; Wang, Y.; Chen, J. Polydopamine Surface Coating Synergizes the Antimicrobial Activity of Silver Nanoparticles. *ACS Appl. Mater. Interfaces* **2020**, *12* (36), 40067−40077.
(37) Zhao, G.; Shi, L.; Yang, G.; Zhuang, X.; Cheng, B. 3D fibrous aerogels from 1D polymer nanofibers for energy and environmental applications. *J. Mater. Chem. A* **2023**, *11* (2), 512−547.
(38) Cai, C.; Liu, Y.; Li, L.; Dong, T.; Chen, W.; Zhou, Z.; Li, Q.; Sun, Y.; Peng, W.; Wang, J.; Nie, S.; Li, X. Wet-resistant, dustproof, and germproof self-powered lignocellulosic triboelectric filters for respiratory protection, monitoring, and diagnosis. *Chem. Eng. J.* **2023**, *476*, 146819.
(39) Babu, A.; Aazem, I.; Walden, R.; Bairagi, S.; Mulvihill, D. M.; Pillai, S. C. Electrospun nanofiber based TENGs for wearable electronics and self-powered sensing. *Chem. Eng. J.* **2023**, *452*, 139060.
(40) Wang, D.; Zhang, D.; Chen, X.; Zhang, H.; Tang, M.; Wang, J. Multifunctional respiration-driven triboelectric nanogenerator for self-powered detection of formaldehyde in exhaled gas and respiratory behavior. *Nano Energy* **2022**, *102*, 107711.
(41) Hsu, L.-F.; Natarajan, K.; Karuppiah, C.; Yang, C.-C. Green reduction and uniform assembly of silver nanoparticles on polydopamine functionalized sulfur-doped graphitic carbon nitride nanosheets for highly sensitive H2O2 detection via nonenzymatic approach. *Colloids Surf., A* **2023**, *677*, 132383.
(42) Mohan, V.; Mariappan, V. K.; Pazhamalai, P.; Krishnamoorthy, K.; Kim, S.-J. Unravelling the impact of carbon allotropes in flexible polydimethylsiloxane film towards self-powered triboelectric humidity sensor. *Carbon* **2023**, *205*, 328−335.
(43) Zhao, K.; Li, R.; Qi, W.; Tian, X.; Zhang, Z.; Wang, Y.; Zhang, Y.; Zhang, H.; Wang, W. Adjustable strength and toughness of dual cross-linked nanocellulose films via spherical cellulose as soft-phase. *Carbohydr. Polym.* **2024**, *327*, 121708.
(44) Popović, M.; Novaković, M.; Pjević, D.; Vaňa, D.; Jugović, D.; Tošić, D.; Noga, P. Investigating on the microstructure and optical properties of Au, Ag and Cu implanted TiN thin films: The effects of surface oxidation and ion-induced defects. *J. Alloys Compd.* **2024**, *976*, 173046.
(45) Zhang, N.; Li, J.; Tian, B.; Li, T.; Zhang, J.; Wang, Q.; Zhao, H. RIGP-Induced Surface Modification of Cellulose for the Preparation of Amidoxime-Modified Cellulose/Graphite Oxide Composites with Enhanced Uranium Adsorption. *Ind. Eng. Chem. Res.* **2024**, *63*, 2337−2346.
(46) Nie, P.; Zhao, Y.; Xu, H. Synthesis, applications, toxicity and toxicity mechanisms of silver nanoparticles: A review. *Ecotoxicol. Environ. Saf.* **2023**, *253*, 114636.
(47) Ameen, F.; Al-Homaidan, A. A.; Al-Sabri, A.; Almansob, A.; AlNadhari, S. Anti-oxidant, anti-fungal and cytotoxic effects of silver nanoparticles synthesized using marine fungus Cladosporium halotolerans. *Appl. Nanosci.* **2023**, *13* (1), 623−631.
(48) Attallah, N. G. M.; Elekhnawy, E.; Negm, W. A.; Hussein, I. A.; Mokhtar, F. A.; Al-Fakhrany, O. M. In Vivo and In Vitro Antimicrobial Activity of Biogenic Silver Nanoparticles against Staphylococcus aureus Clinical Isolates. *Pharmaceuticals* **2022**, *15* (2), 194.
(49) Zhang, H.; Zhang, D.; Wang, Z.; Xi, G.; Mao, R.; Ma, Y.; Wang, D.; Tang, M.; Xu, Z.; Luan, H. Ultrastretchable, Self-Healing Conductive Hydrogel-Based Triboelectric Nanogenerators for Human-Computer Interaction. *ACS Appl. Mater. Interfaces* **2023**, *15* (4), 5128−5138.
(50) Zhang, H.; Chen, X.; Liu, Y.; Yang, C.; Liu, W.; Qi, M.; Zhang, D. PDMS Film-Based Flexible Pressure Sensor Array with Surface Protruding Structure for Human Motion Detection and Wrist Posture Recognition. *ACS Appl. Mater. Interfaces* **2024**, *16* (2), 2554−2563.
(51) Wang, N.; Feng, Y.; Zheng, Y.; Zhang, L.; Feng, M.; Li, X.; Zhou, F.; Wang, D. New Hydrogen Bonding Enhanced Polyvinyl Alcohol Based Self-Charged Medical Mask with Superior Charge Retention and Moisture Resistance Performances. *Adv. Funct. Mater.* **2021**, *31* (14), 2009172.
(52) Vazquez-Lopez, A.; Del Rio Saez, J. S.; de la Vega, J.; Ao, X.; Wang, D. Y. All-Fabric Triboelectric Nanogenerator (AF-TENG) Smart Face Mask: Remote Long-Rate Breathing Monitoring and Apnea Alarm. *ACS Sens.* **2023**, *8* (4), 1684−1692.

https://doi.org/10.1021/acsomega.4c01906
ACS Omega 2024, 9, 33643−33651